Hydrostatic Models of Protoplanetary Disks

Christina Walker[1], Kenneth Wood[1], Barbara Whitney[2], J.E. Bjorkman[3]

cw26@st-andrews.ac.uk

Received ______________; accepted ______________

Submitted to the Astrophysical Journal

[1]School of Physics & Astronomy, University of St. Andrews, North Haugh, St Andrews, KY16 9SS, Scotland; cw26@st-andrews.ac.uk, kw25@st-andrews.ac.uk

[2]Space Science Institute, 3100 Marine Street, Suite A353, Boulder CO 80303, USA

[3]Ritter Observatory, Department of Physics & Astronomy, University of Toledo, Toledo OH 43606, USA

ABSTRACT

We present Monte Carlo radiation transfer models of protoplanetary accretion disks that are assumed to be in vertical hydrostatic equilibrium. Our models are multi-dimensional, conserve flux exactly, and include multiple anisotropic scattering. We compare the results of our code to other recent disk models and report some differences in interpretation, disk temperature structure, and the emerging spectra.

For disks with a steady accretion rate, irrespective of the total optical depth (mass) of the disk, we do not find significant shadowing of the outer disk by the inner edge. We show that spectral energy distribution models of fixed density disks (with scaleheights that are parameterized by a single power law over their entire radius) give a good match with hydrostatic disks. Low IR excess emission observed in the far-IR SEDs of some sources has been attributed to self-shadowing of the disk, but the assumed disk surface density and any dust settling have a greater impact on the SED shape.

Our two dimensional radiation transfer models exhibit some differences in the disk temperature structure compared to models that treat the disk as a series of plane parallel annuli. Two dimensional radiation transfer results in disk temperatures that are 10% to 20% higher than vertical-only radiation transfer models. These temperature differences, which arise from radial transport effects not present in vertical-only models, do not lead to significant variations in the hydrostatic structure since the disk scaleheight is proportional to $\sqrt{T}$. They do, however, lead to factors of two difference in the predicted fluxes at mid to far-IR (30μm to 300μm) wavelengths. Modeling SEDs in this wavelength regime is known to be very sensitive to disk flaring and dust settling.

As an example of our code, we show that we can successfully model the

SED and high resolution scattered light images of the near edge-on disk around HH30 IRS with a steady accretion disk in vertical hydrostatic equilibrium with dust and gas well-mixed.

Subject headings: radiative transfer

1. Introduction

Circumstellar disks are seen as a natural step in the formation of low mass stars (e.g., Shu et al. 1987). Since they were first identified through their signature infrared excess emission (e.g., Mendoza 1968) there have been many observational and theoretical investigations into their properties, evolution, and lifetimes. In very general terms, typical disks surrounding classical T Tauri stars and Herbig Ae stars have radii of a few hundred AU, masses in the range 10^{-4} to $10^{-1}\,M_{\odot}$, and accretion rates of 10^{-9} to $10^{-6}\,M_{\odot}\,\mathrm{yr}^{-1}$ (e.g., see review in PPIV part II 2000). Disks that are heated by starlight and dissipation of viscous accretion have scaleheights that increase with radial distance from the star, (e.g., Kenyon & Hartmann 1987) and this natural flaring can explain many of the observed spectral energy distributions (SEDs). If dust and gas are well mixed throughout the disk and there has not been significant dust settling, flared disks viewed close to edge-on will block direct starlight and become visible in scattered light (Whitney & Hartmann 1992). High resolution images from *Hubble Space Telescope* and ground based telescopes have detected many such scattered light disks (e.g., Burrows et al. 1996; Padgett et al. 1999; Grosso et al. 2003). Coronagraphic techniques have also allowed the detection of scattered light disks where the central star is revealed (e.g., Weinberger et al. 2002; Krist et al. 2003, 2005; Schneider et al. 2003).

Building on from the first theoretical SED models of flared disks (Kenyon & Hartmann

1987), there have been increasingly sophisticated techniques to study the disk temperature structure and emergent spectra. Models by Calvet et al. (1991) showed the temperature inversion that occurs in the disk where the upper layers, that are heated by starlight, are warmer than the disk interior. Their radiation transfer in the disk is 1D in the vertical direction and they treat the disk as a series of plane parallel annuli. This approach was extended to calculate the structure of steady accretion disks by D'Alessio et al. (1998, 1999, 2001). The hot upper layers of the disk and cooler interior were incorporated into the two layer model of Chiang & Goldreigh (1997, 1999). Two dimensional radiation transfer techniques for disk models include Monte Carlo (Wood et al. 2002; Whitney et al. 2003; Wolf 2001; Kurosawa et al. 2004), and traditional radiation transfer techniques (e.g., Nomura 2004; Steinacker et al. 2004; Dullemond 2002). Pascucci et al. (2004) compared several codes and presented benchmark test cases for the temperature structure and SED from a disk with a prescribed density heated by starlight alone.

Usual assumptions are that the disks are geometrically thin, $h(R)/R < 1$, they are in vertical hydrostatic equilibrium, and dust and gas are coupled (e.g., Kenyon & Hartmann 1987; Chaing & Goldreich 1997, 1999; D'Alessio et al. 1998, 1999, 2001; Dullemond 2002). Such models that solve for the disk structure have shown various effects including extended upper layers of the disk (D'Alessio et al. 1998) and possible shadowing of the outer disk by the disk's inner edge (Dullemond 2002; Dullemond & Dominik 2004). We have recently extended our Monte Carlo codes to iteratively solve for the disk structure assuming vertical hydrostatic equilibrium and have modeled disks around brown dwarfs (Walker et al. 2004) and T Tauri stars (Akeson et al. 2005; O'Sullivan et al. 2005).

This paper compares our code to other recent disk structure models and points out some differences in the temperature and SED due to multi-dimensional radiation transfer effects. We also show that the disk structure and emergent SEDs and images of passive disks in hydrostatic equilibrium are well reproduced using disks wheere the density structure can be described using simple radial power laws for the scaleheight and surface density. This means that SEDs and images from hydrostatic disks can be simulated quickly without using the exact and more CPU-intensive iterative models to determine disk structure and emergent spectra. The general recipe we present linking hydrostatic and "power law" disks will be very useful for modeling data using our publicly available radiation transfer codes. For data that do not match SEDs using our general recipe for hydrostatic disks, we give suggestions on how to modify the disk structure to investigate dust settling. Based on our hydrostatic and power law disk models, we discuss the relative importance on global disk structure of shadowing of the outer disk by the inner edge of the disk.

The layout of the paper is as follows: Section 2 describes our Monte Carlo code. §3 presents results of our code and addresses the issue of disk shadowing. §4 compares our code with approximate radiation transfer techniques. In §5 we apply hydrostatic disk models to the SED and images of the near edge-on disk around HH30 IRS, and §6 presents a summary of our findings.

2. Monte Carlo Radiation Transfer Code

Our Monte Carlo codes that simulate radiation transfer in dusty systems have evolved over the last fifteen years starting from the scattered light models of protostellar disks and envelopes of Whitney & Hartmann (1992). Our codes now include radiative equilibrium techniques that solve for the dust temperature structure and emergent multi-wavelength images and spectra (Bjorkman & Wood 2001), the inclusion of a diffusion approximation for the most dense regions towards the disk midplane (Bjorkman et al. 2003), and more recently the self-consistent determination of the structure of disks that are in vertical hydrostatic equilibrium (Walker et al. 2004). Our codes includes multiple anisotropic scattering and conserve flux exactly. The original Bjorkman & Wood (2001) technique calculated the temperature based on the number of photons absorbed in a given grid cell. We have updated our codes as described in Walker et al. (2004) to also calculate temperatures using the path-length formula (Lucy 1999) for determining mean intensities and absorbed energy. The path-length technique provides higher signal-to-noise in the temperature determination and allows for temperature calculations in very optically thin cells. Our code produces temperature grids calculated using both the path-length and original Bjorkman & Wood (2001) techniques. Using the temperature calculated with the Bjorkman & Wood (2001) technique allows us to easily see where photons have been absorbed in the disk and subsequently contribute to the thermal SED. We will show temperature plots using both techniques in this paper and use them in our discussion of flaring disks.

Recent work has shown that accurate disk SED models must include reprocessing of stellar radiation at the inner edge of the disk (Natta et al. 2001; Dullemond et al. 2001). Monte Carlo techniques account for these multi-dimensional radiation transfer effects without simplifications and our code naturally calculates the temperature structure of the inner edge and the reprocessing of photons there. We refer the reader to our papers above for code details. Although the results presented in this paper are for axisymmetric disks, the Monte Carlo radiation transfer technique is intrinsically three dimensional and readily extendable to more complex systems (Indebetouw et al. 2005, in preparation).

We have benchmarked our Monte Carlo code against the fixed density disk models in (Pascucci et al. 2004) and against several other independently developed codes that solve for vertical hydrostatic equilibrium in the disk. Our models are in excellent agreement with all the multi-dimensional codes we have compared with. A future paper will present results of benchmarking for hydrostatic equilibrium disks (Schegerer et al. 2005, in preparation). The following presents results obtained with our code.

3. Comparison of Hydrostatic and Fixed Density Disks

The major source of heating in disks around CTTs and Herbig Ae stars is radiation from the central star. In CTTs heating by viscous accretion is also important for modeling SEDs, but in Herbig Ae disks this is generally considered to be very small and often ignored (e.g., Dullemond et al. 2001; Muzerolle et al. 2004). §3.1 presents models for CTTs and Herbig Ae stars that include heating from starlight and accretion. §3.2 and §3.3 then investigate disk models where the heating source is only starlight and the boundary condition for the disk structure is that a fixed power law is assumed for the radial variation of disk surface density.

Disks are not vertically isothermal, so at any given radius their vertical structure cannot be described with a unique scaleheight. However, a question we address here is can disks with scaleheights and surface densities parameterized by simple radial power laws reproduce the SEDs of hydrostatic disks? This is important because computing the SED and modeling data using a fixed density model is faster than iterating towards a self-consistent solution for the disk density and temperature structure.

3.1. Steady Accretion Disks in Hydrostatic Equilibrium

Figure 1 shows the SEDs for disks of different masses (accretion rates) surrounding CTTs and Herbig Ae stars heated by starlight and dissipation of viscous accretion. Figure 2 shows the temperature and density structure for the accretion disks of mass $M_d = 10^{-4} M_{\odot}$. The models are for irradiated, steady accretion disks around a CTTs and Herbig Ae star with stellar parameters, disk masses, and accretion rates summarized in Table 1. All model disks have an outer radius of 200 AU and an inner radius set by the dust destruction temperature, assumed to be 1600K. We make the same assumptions as D'Alessio et al.

(1998) that there is a steady accretion rate through the disk and the disk is in vertical hydrostatic equilibrium. The disk viscosity is described using the α prescription of Shakura & Sunyaev (1973) and we assume a value of $\alpha = 0.01$ as suggested by Gullbring et al. (1998) and Hartmann et al. (1998). The disk radial surface density in a steady α accretion disk can be approximated by,

$$\Sigma(R) = \frac{\dot{M}}{3\pi\alpha}\frac{\Omega}{kT_c}\mu m_H\left[1 - \left(\frac{R_\star}{R}\right)^{1/2}\right] \tag{1}$$

where R is cylindrical radius, $\Omega = \sqrt{GM/R}$ is the keplerian angular velocity, k is the Boltzmann constant, μ is mean molecular weight (we adopt μ=2.3 for a hydrogen/helium mixture) and m_H is the mass of a hydrogen atom. The midplane temperature is T_c and in our iterative radiation transfer/hydrostatic equilibrium procedure we initially approximate this using $T_c = T_0(R/R_\star)^{0.5}$ where,

$$T_0 = \frac{\mu m_H G M_\star}{k R_\star^3} h_0^2 \tag{2}$$

where G is Newton's constant and h_0 is an initial guess for the scaleheight at the stallar surface, and we usually use $h_0 = 0.01R_\star$. Given a surface density profile it is then possible to calculate the disk mass by summing up the contributions of mass at each radius from R_{in} to R_d,

$$M_d = 2\pi \int_{R_{in}}^{R_d} \Sigma_\infty \; R \; dR \tag{3}$$

For a given accretion rate and a calculated disk mass, the accretion contribution to the flux at radial distance R is (Pringle 1981):

$$F_{accn} = \frac{3GM_*\dot{M}}{8\pi} R^{-3} \left[1 - \left(\frac{R_*}{R}\right)^{1/2}\right] \quad (4)$$

For the radiation transfer simulation, the opacity in the disk is dominated by dust. In the simulations of Figs. 1 and 2, the dust model is one we have used to fit the SEDs of several CTTs and brown dwarf disks (Wood et al. 2002; Rice et al. 2003; Walker et al. 2004; O'Sullivan et al. 2005). The wavelength dependence of the absorption and scattering properties of this dust model are shown in Wood et al. (2002).

The SEDs in Fig. 1 show the characteristic infrared excess due to reprocessing of starlight and heating from viscous accretion. For edge-on viewing the SED is double peaked with scattered light at short wavelengths and thermal reprocessing at long wavelengths: see Fig. 9 in Wood et al. (2002) for the component parts of the SED (direct starlight, scattered starlight, accretion energy, and reprocessed thermal radiation). As the disk accretion rate is decreased, the total disk mass is decreased as is the heating from viscous accretion, so the IR excess falls.

As with D'Alessio et al. (1998), we find that at large radii the disk scaleheight (taken from the midplane temperature) and the surface density scale roughly as $R^{5/4}$ and R^{-1} respectively. In Fig. 2 the density and temperature structure show that the inner edge of the disks shield material just beyond it. This results in a rapid drop in the temperature so that the inner edge appears more vertically extended than radii just beyond it. The temperature structure shows the hot upper layers that intercept direct stellar radiation and lie at around three to five scaleheights above the midplane. The temperature plots, using the Bjorkman & Wood (2001) technique, show where stellar and thermal disk photons are absorbed and reprocessed contributing to the infrared excess SED. Note the model Herbig Ae disk is less flared than the CTTs disk due to the larger gravity of the higher mass star. For comparison, hydrostatic equilibrium disks around brown dwarfs are more flared due to the lower gravity of the central star (Walker et al. 2004). The disks in Fig. 2 are seen to flare over their entire extent and the inner edge does not cast a significant shadow so as to cause any extreme effects such as collapse of the outer disk (e.g., Bell et al. 1997; Dullemond 2002; Dullemond & Dominik 2004). We will discuss this further in §3.3.

3.2. Hydrostatic Passive Disks using Power Laws

When the heating is dominated by starlight and accretion is negligible, the disk structure is solved by enforcing vertical hydrostatic equilibrium with boundary conditions that the total mass is constant and the surface density has a prescribed radial power law, $\Sigma(R) \sim R^{-p}$. Disk surface density gradients are ususally in the range $1 \leq p \leq 2$, with $p = 3/2$ the value quoted for the minimum mass solar nebula (Hayashi 19XX) and $p \approx 1$ found for irradiated steady accretion disks (D'Alessio et al. 1998). This section addresses the following question: *Can we reproduce the SEDs of disks in vertical hydrostatic equilibrium using disks where the surface density and scaleheight are described with a simple radial power laws?* If so, this will allow pre-computed libraries of SEDs for fixed density disks to be used to fit real data and estimate disk properties. Once the disk properties have been estimated in this fashion, more detailed modeling can be done of individual sources using hydrostatic models which take longer to compute.

Figure 3 compares SEDs for hydrostatic with those for power law disks with masses $10^{-2} \leq M_d/M_\odot \leq 10^{-8}$. The power law disks have the parameterized density structure,

$$\rho = \rho_0 \exp\left[\frac{-z^2}{2h(R)^2}\right]\left(\frac{R_{dust}}{R}\right)^{\alpha} \tag{5}$$

where the scaleheight $h(R) = h_{dust}(R/R_{dust})^{\beta}$. In this model the surface density is $\Sigma \sim R^{-p}$

where $p = \alpha - \beta$.

The SEDs shown in Fig. 3 that were produced using power-law disks have a simple prescription where we set $\beta = 1.25$, the radial density exponent is $\alpha = \beta + p$, and $h(R)$ is scaled from the dust destruction radius, $h_{dust}/R_{dust} = c_s/\ \Omega(R_{dust})$, where $c_s = \sqrt{kT/\mu m_{\rm H}}$ and $T = 1600$ K at the dust destruction radius. The dust destruction radius in disks heated by starlight when accretion is negligible is well approximated by $R_{\rm dust}/R_\star = (T_{\rm dust}/T_\star)^{-2.085}$, where $T_{\rm dust} = 1600$ K in our models (Whitney et al. 2005). The value $\beta = 1.25$ in this prescription is not unexpected, because irradiated disks tend to have a temperature structure $T(R) \propto R^{-0.5}$, which gives a scaleheight $h(R) \propto R^{1.25}$.

Figure 3 shows that a power-law disk with a density given by equation (5) with surface densities and scaleheights given by the above recipe, can reproduce the SED of p=1 hydrostatic disks for low inclinations. At high inclinations fixed density disks have lower flux levels for the same viewing angle. If the disk flaring (β) or fiducial scaleheight (h_{dust}) is varied we can get better agreement, however we believe the prescription we have described provides a good match for initial studies and will only result in small errors of a few degrees at inclinations where the star becomes obscured in the optical (generally $i > 70^\circ$, but depends on disk mass). As with all SED fitting we should be cautious since these are idealized models of smooth, axisymmetric disks and real disks are likely to exhibit 3D density structures and may not be in strict hydrostatic equilibrium due to dust settling or dynamical effects such as disk warping.

The general recipe described above for power-law disks with $1 \le p \le 2$ also reproduces the SEDs of hydrostatic disks surrounding hotter ($T_\star \sim 20000$ K) and cooler ($T_\star \sim 4000$ K) stars. This general recipe relating the SEDs of hydrostatic and power-law disks therefore allows us to use non-iterative radiation transfer codes to compute SEDs and images for disks with density structures given by equation (5). Using a non-iterative code is faster than iterating towards a self-consistent solution for the temperature and density structure in an irradiated disk. In practice this recipe could be used as follows. Given SED data for a disk system, use a non-iterative radiation transfer code, a disk structure given by equation (5), and our recipe for the disk scaleheight described above. If the model SED and observations match, then the implication is that the disk is in vertical hydrostatic equilibrium with dust and gas well-mixed. If the simulation does not match the observations, then depending on the discrepancy in the mid-IR (10μm $\lesssim \lambda \lesssim 100\mu$m) a couple of effects not included in passive disk models may be important. If the model SED has a lower mid-IR flux than observed, then disk heating from viscous accretion may be important. For high accretion rates, disk heating from viscous dissipation manifests itself most prominently by raising the mid-IR emission (e.g., D'Alessio et al. 1998). If, on the other hand, the simulated mid-IR flux is higher than observed, it is possible that dust settling is dominating the disk shape. In this case, a less flared disk may better fit the observations and this may be achieved by changing the parameters h_{dust} and/or β to change the disk shape. These are only general suggestions on how to tackle SED modeling and obviously there is a very wide parameter space, including the effects of different scaleheights for different dust sizes. However, parameterizing the disk using equation (5) and the general recipe described, quickly allows us to determine whether the observations are consistent with hydrostatic disks and to investigate the role of accretion and/or dust settling in fitting disk SEDs.

3.3. Passive Disks: Effects of Disk Mass, Surface Density, and Self-Shadowing

In this section we discuss the role of disk mass, surface density, and the inner edge in determining the large scale disk structure. Recent models of disks in hydrostatic equilibrium with dust and gas well coupled (Dullemond & Dominik 2004) suggest that disks with steep surface densities or very low total mass result in a new class "self-shadowed" disks. For disks with steep surface density gradients (e.g., $p = 4$), the infrared flux is lower than disks of the same total mass, but with shallower surface density exponents ($p = 1$). The mm flux levels are comparable between the $p = 1$ and $p = 4$ model disks. The shape of the SED and temperature structure of these steep surface density disks, led Dullemond & Dominik (2004) to conclude that the inner edge of the disk casts a shadow on the outer disk, shielding it from direct stellar heating, and thus resulting in a disk structure that is flatter than $p = 1$ disks. Models with a very small total disk mass also exhibit small IR excesses and their temperature structure was also interpreted as being self-shadowed. Of course, optical depth effects will lead to all disks having regions that are shielded from direct stellar irradiation. A result is that dust grains in the disk midplane have lower radiative equilibrium temperatures than grains at the same location that are directly exposed to stellar radiation. This has been explored as a means of moving the "snow-line" (Hayashi??) to smaller radii in disks (e.g., Sasselov & Lecar 19XX). The models of Dullemond & Dominik (2004) take this shadowing effect further and suggest a new class of disks where shadowing by the inner edge dominates the structure in the outer regions of the disk. The cartoons in Dullemond & Dominik (2004) illustrate this interpretation, suggesting that the inner edge of the disk may be significantly "puffed up" compared to material behind it, and the inner edge strongly influences the structure of the outer disk.

Low infrared excess emission is a general feature of flat disks and also those with steep radial surface densities and/or low mass. We will show this feature of low infrared excess is present in the SEDs of both hydrostatic and fixed density disks. In what follows we compare and discuss the structure and SEDs of hydrostatic and fixed density disks with varying radial surface density gradients in an attempt to determine the relative importance of inner edge effects on the global disk structure. Our models differ from Dullemond & Dominik (2004) in that we include scattering, whereas they set scattering opacity to zero. We adopt ISM grains, KMH (Kim et al. 1994), which have a wavelength-dependent opacity similar to those used by Dullemond & Dominik (2004).

3.3.1. Disk Mass

We have shown in the previous section that hydrostatic disks with radial surface density exponents in the range $1 \leq p \leq 2$ can be well approximated by the power-law disks described by equation (5) and using our recipe for the disk scaleheight. In this prescription, the disk scaleheight is a monotonically increasing function of radius. The recipe applies over a wide range of disk masses, so our interpretation of low mass hydrostatic disks is that it is the disk mass that determines the SED shape and not any shadowing effects caused by the inner edge of the disk. Low mass disks also have very low surface brightnesses in scattered light and thermal images, which we again interpret as due to the small mass of disk material and not because of inner edge shadowing effects.

3.3.2. Disk Surface Density

We have shown in §3.2, that the SEDs of $p = 1$ hydrostatic disks can be reproduced with power law disks whose scaleheights monotonically increase with distance from the star so that the disk surface is always concave upwards and capable of receiving radiation directly from the star. This suggests that the small shadowing directly behind the inner edge of these disks has no significant impact on the far-IR SED or the structure of the outer disk. However, Fig. 4 shows that it is not possible to use power-law disks with the above recipe for h_{dust} and $\beta = 1.25$ to reproduce the SEDs of hydrostatic $p = 4$ disks. We find that h_{dust} must be reduced by about XX% for power-law disks to match hydrostatic models, indicating that inner edge effects are important for the global disk structure in disks with very steep surface densities. Note, however, that using our prescription for h_{dust}

and β, the infrared excess is lower than that for a $p = 1$ disk of the same total mass. This indicates that the disk surface density has a big effect on determining how much radiation may be reprocessed in the disk. Steep surface densities move the disk mass to smaller radii, so that the cooler, outer disk regions will contribute less to the infrared excess. Therefore, the surface density gradient influences the SED, but for very steep gradients shadowing by the inner edge also plays a role in determining the structure of the outer disk.

Another way to look for evidence of shadowing is to study temperature cross-sections of the disks. The upper panels in Fig. 6 show 2D maps where the temperature is calculated at all points, including where the medium is optically thin and does not contribute any emission. These figures clearly show that $p = 1$ disks exhibit flared surfaces, whereas the $p = 4$ disk does appear to be isothermal and in the shadow of the inner edge. A more instructive way to examine the temperature structure is, however, to plot the temperature only where photons are absorbed and are reprocessed into the disk thermal spectrum (see Fig. 6, middle panels). The resulting temperature maps show that the $p = 4$ disk does in fact exhibit a flared surface. These 2D temperature plots suggest these disks are not self-shadowed at the levels suggested by the illustrations presented by Dullemond (2002) and Dullemond & Dominik (2004).

In summary, our results for the disk temperature/density structure and SED are in agreement with those of Dullemond & Dominik (2004), but we differ slightly in our interpretation. While the inner edge of the disk is important for determining the near-IR excess (Natta et al. 2001; Dullemond et al. 2001) and the photopolarimetric variability in magnetically accreting CTTs (Bouvier et al. 1999; Ménard et al. 2003; O'Sullivan et al. 2005), our interpretation of the models here (and similar models presented in other publications) is that it does not significantly affect the height of the irradiation surface. Although minimal shadowing of the outer disk by the inner edge may occur it only influences the disk structure for disks with very steep radial surface density gradients.

Indeed, this effectively is the conclusion of Dullemond & Dominik (2004) who investigated the difference between SEDs of Type I and II Herbig AeBe stars. Type I and II sources have similar mm flux levels and therefore similar disk masses, but Type II sources have lower infrared excesses than Type I. Models that reproduce the SED features of Type I have flaring surfaces, $\Sigma \sim R^{-1}$, and $M_{dust} \geq 10^{-3} M_{\odot}$. Dullemond & Dominik (2004) note that because of their similar mm flux levels, Type II sources are unlikely to have less massive disks than Type I and therefore require models with $\Sigma \sim R^{-4}$ or very flat disks where large dust grains have settled to the midplane. Therefore, the low levels of infrared excess emission observed in some sources are probably attributable to dust settling.

4. Comparison with Vertical-Only Radiation Transfer Models

As stated in §2, a future paper will compare our hydrostatic disk structure calculations with other two dimensional codes. This section compares our hydrostatic disk models (using our iterative code and not the power-law disk recipe) with the resulting temperature and density structure and SEDs from the disk models of D'Alessio et al. (1998, 1999, 2001).

The disk models of D'Alessio et al. (1998, 1999, 2001) and the associated grid of models available via the WWW (D'Alessio et al. 2005) adopt a vertical-only approximation for radiation transfer within the disk. In their models the disk is heated by starlight and the dissipation of viscous accretion, the disk is divided into concentric plane-parallel annuli, and stellar radiation impinges the disk irradiation surface at an oblique angle. Figure 7 compares our models with the fiducial disk model of D'Alessio et al. (1999). This model has $R_{\star} = 2R_{\odot}$, $M_{\star} = 0.5M_{\odot}$, $T_{\star} = 4000$ K, $R_d = 300$ AU, and a steady accretion rate of $\dot{M} = 10^{-8} M_{\odot}$ yr^{-1}. The dust opacity is that of ISM grains as in D'Alessio et al. (1999)

and for the purposes of comparison we assume isotropic scattering in the Monte Carlo simulations.

Comparing the models we find that the temperature calculated with our code is consistently higher by about 10% to 20%. The temperature differences do not lead to big differences in the computed density structures, since the disk scaleheight is proportional to $\sqrt{T}$. The comparison of the vertical density cuts, in Fig. 7, at different radii shows that the disk structure calculations are in good agreement. The higher temperatures in our calculations do, however, lead to a difference in the flux levels at mid to far-IR wavelengths ($20\mu\mathrm{m} \lesssim \lambda \lesssim 300\mu\mathrm{m}$) as can be seen in Fig. 8. The higher temperatures in our calculations are a two-dimensional radiation transfer effect that manifests itself most prominently in the long wavelength flux discrepancies. The temperature difference arises because photons that are reprocessed in the disk can heat other disk regions. Therefore radial transport, which is not accounted for in vertical-only models, is important for determining accurate temperatures in the disk and the correct flux in the $20\mu\mathrm{m} \lesssim \lambda \lesssim 300\mu\mathrm{m}$ range.

We confirmed that radial transport is the reason for the discrepancies between the two codes by modifying our Monte Carlo code so photons reprocessed in the disk are re-emitted either straight up or straight down (with a 50% probability of up/down), thus simulating vertical-only radiation transport of the disk radiation field. Compared to the correct isotropic re-emission code, this vertical-only approximation in our Monte Carlo code results in lower temperatures and lower mid and far-IR fluxes at the same levels seen in Fig. 8.

5. Modeling The Disk Around HH 30 IRS

The above sections presented theoretical calculations for the structure and SED of disks that are assumed to be in vertical hydrostatic equilibrium with dust and gas well mixed throughout. An obvious question is do these models and assumptions reproduce observations of real disks? Many disks can be modeled with these assumptions (e.g., Chaing & Goldreich 1999; Natta et al. 2000, 2001), while some disks do appear to require less flaring to match the SEDs and scattered light images, likely due to dust settling or surface density effects (e.g., Chaing et al. 2001; Dullemond & Dominik 2004). Images of edge-on disks seen via scattered light, provide an excellent test of the model assumptions and perhaps the best studied edge-on disk is that associated with HH 30 IRS (Burrows et al. 1996). Two groups have studied the multiwavelength images (Burrows et al. 1996; Wood et al. 1998; Cotera et al. 2001; Watson & Stapelfeldt 2004), variability (Wood & Whitney 1998; Stapelfeldt et al. 1999; Wood et al. 2000), and SED (Wood et al. 2002) of this system using the parametrized fixed density models of Eqn 5. Broad agreement is found on the disk mass ($M_d \sim 10^{-3} M_\odot$), size ($R_d \sim 200$ AU), and scaleheight ($h[100\mathrm{AU}] \sim 15$ AU). Modeling of multiwavelength images and the sub-mm SED indicate the circumstellar dust has a grayer opacity and hence a larger average grain size than interstellar grains. We have modeled the HH 30 IRS disk with our new iterative code assuming steady accretion and vertical hydrostatic equilibrium. The dust model is the same as that presented in Wood et al. (2002) and dust and gas are assumed to be well mixed in the disk. A model fit, for a disk inclined at 81°, is shown in Figs. 9 – 10. This model has $R_\star = 1.5 R_\odot$, $M_\star = 0.64 M_\odot$, $T_\star = 3500$ K, $R_d = 250$ AU, and a steady accretion rate of $\dot{M} = 2 \times 10^{-9} M_\odot$ yr^{-1}, giving $M_d = 3 \times 10^{-3} M_\odot$. Future *Spitzer Space Telescope* observations at far-IR wavelengths will provide additional constraints on the disk structure and dust model.

6. Summary

We have compared our Monte Carlo radiation transfer models for disks in hydrostatic equilibrium with other recent disk models. Our main findings are the following.

- Fixed density disks with scaleheights that are parameterized by a single power law can reproduce the SEDs and images of disks where the detailed structure has been solved for. A general prescription for $\Sigma \sim R^{-1}$ disks is formulated in $3.1.

- Like recent models, we find that the inner edge of the disk casts a shadow on outer disk regions. The shadowed region is, however, very small and disk radial surface density or dust settling are the dominant controls on the shape of the far-IR SED. Unless disks are very low mass and have steep surface density profiles, shadowing by the inner edge is not responsible for producing the small IR excesses seen around some Herbig Ae stars.

- Two dimensional radiation transfer gives disk temperatures that are 10% to 20% higher than models that employ vertical-only transport in the disk. This does not lead to big differences in the disk structure, but it does result in vertical-only models producing a factor of two less flux at mid to far-IR wavelengths.

The models presented in this paper are for two-dimensional smooth density disks and highlight differences in computed observable fluxes compared to approximate radiation transfer techniques. In reality the circumstellar environment is unlikely to be smooth or two-dimensional and therefore three dimensional disk models need to be investigated. Already it has been shown that 3D circumstellar geometries can influence the optical through mid-IR fluxes and the shape and strength of the silicate emission/absorption features at 10μm and 20μm (Whitney et al. 2005). High resolution mid-IR spectroscopy is now returning very detailed spectra enabling the discrimination of amorphous and crystalline features in disks (e.g., Acke & van den Ancker 2004; Kessler-Silacci et al. 2005). Therefore, to be confident of the interpretation of the disk chemistry from such observations, 3D disk models are required.

We acknowledge funding for this work from the UK PPARC (KW and CW), NASA LTSA (BW), and the NSF (BW and JB). Paolo D'Alessio kindly provided the results of her simulations in electronic format for the comparisons presented in §4.

Table 1. Accretion Disk Model Parameters

$T_\star$ (K)	$M_\star$ ($M_\odot$)	$R_\star$ ($R_\odot$)	$\dot{M}$ ($M_\odot yr^{-1}$)	M_d ($M_\odot$)
4000	0.5	2	5×10^{-9}	10^{-2}
4000	0.5	2	6×10^{-11}	10^{-4}
4000	0.5	2	6×10^{-13}	10^{-6}
10000	2.5	2	5×10^{-9}	10^{-2}
10000	2.5	2	6×10^{-11}	10^{-4}
10000	2.5	2	7×10^{-13}	10^{-6}

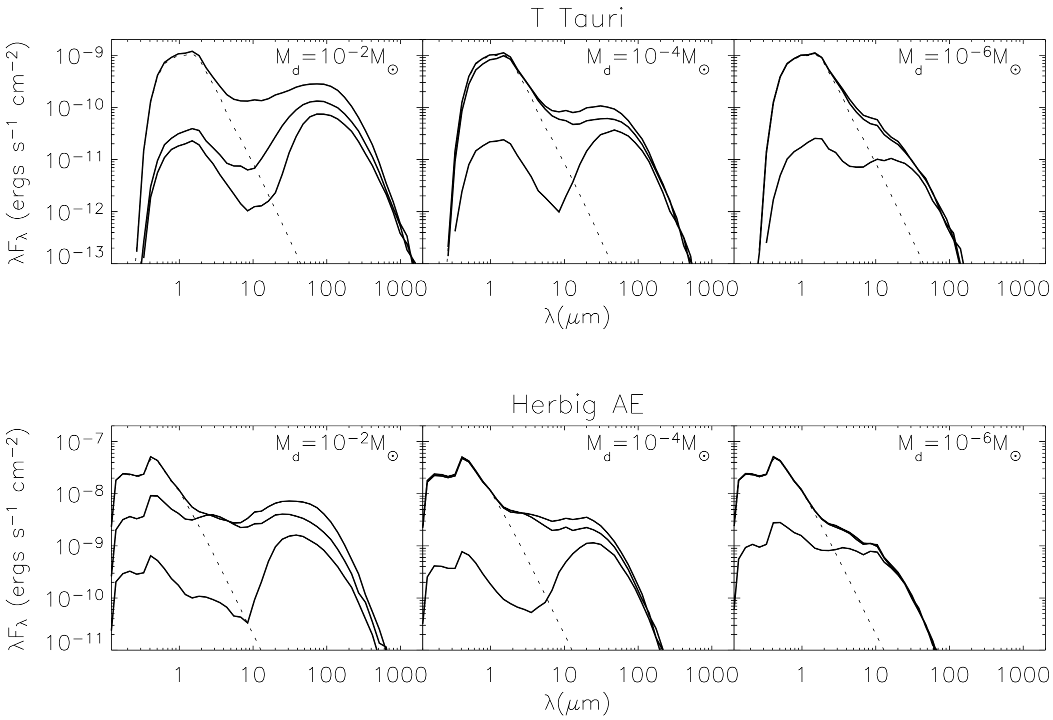

Fig. 1.— SEDs for hydrostatic disks at inclinations of $10°, 60°$ and $85°$. Disk mass indicated in plots and accretion rates are: (a)$\dot{M} = 5 \times 10^{-9} M_\odot$ yr^{-1}; (b)$\dot{M} = 6 \times 10^{-11} M_\odot$ yr^{-1}; (c)$\dot{M} = 7 \times 10^{-13} M_\odot$ yr^{-1}.

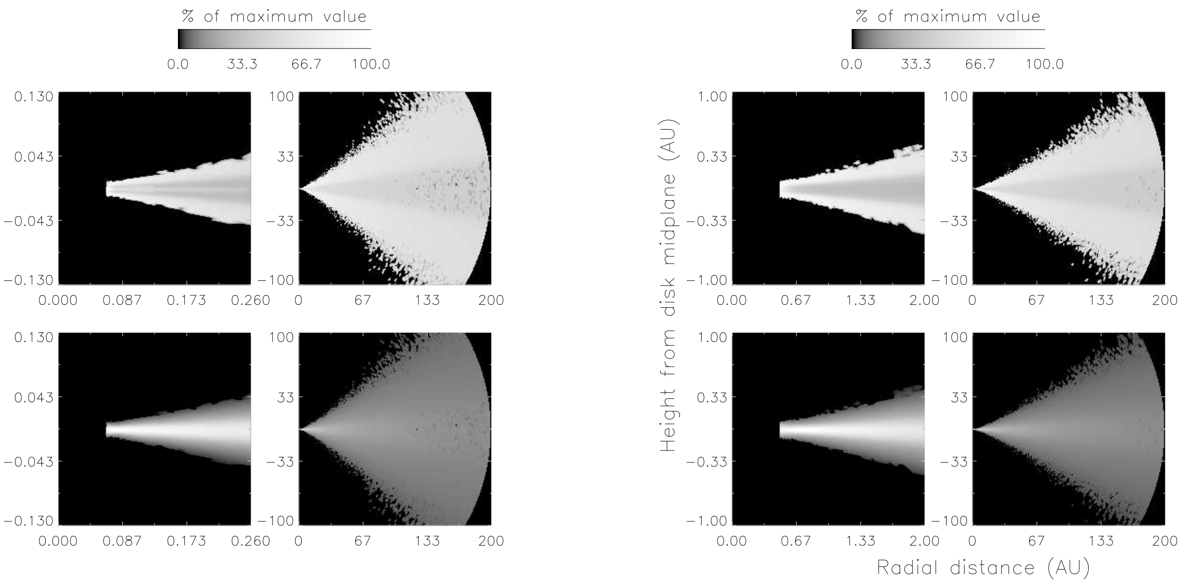

(a) (b)

Fig. 2.— Contour plots showing 2D temperature and density slices on two sizescales for vertical hydrostatic disks of mass $M_d = 10^{-4} M_\odot$ around: (a) a T Tauri star with $M_\star = 0.5 M_\odot$, $R_\star = 2 R_\odot$, $T_\star = 4000K$; (b) a Herbig AE star with $M_\star = 2.5 M_\odot$, $R_\star = 2 R_\odot$, $T_\star = 10000K$. HAe disk is less flared due to larger gravity of the central star.

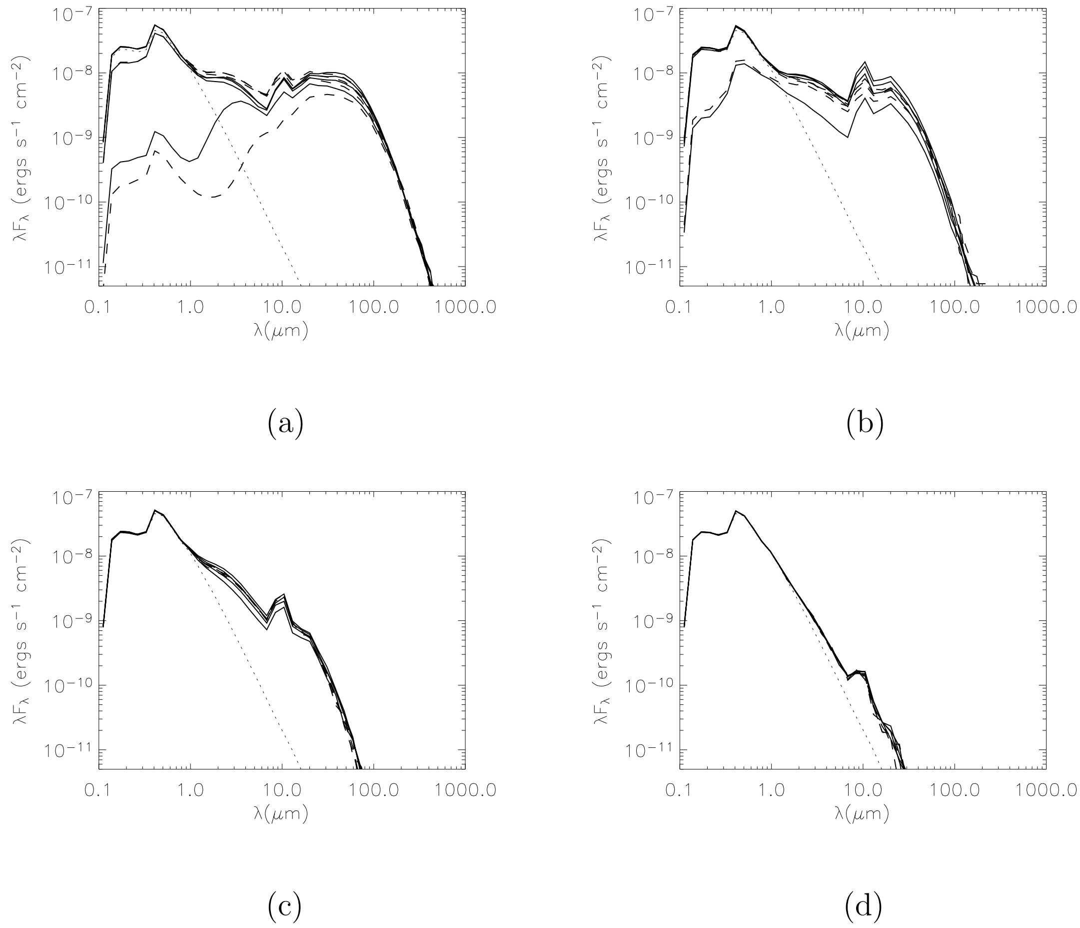

Fig. 3.— SEDs for $p = 1$ disks of varying mass at inclinations of $72.5 - 75.5°, 60.0 - 63.3°, 45.6 - 49.5°$, and $25.8 - 31.8°$. Hydrostatic models are shown as solid lines and fixed density models as dashed lines. Fixed density models have $h_{dust} = 0.036 R_\star$ and $\beta = 1.25$. Disk masses are: (a) $10^{-2} M_\odot$; (b) $10^{-4} M_\odot$; (c) $10^{-6} M_\odot$; (d) $10^{-8} M_\odot$.

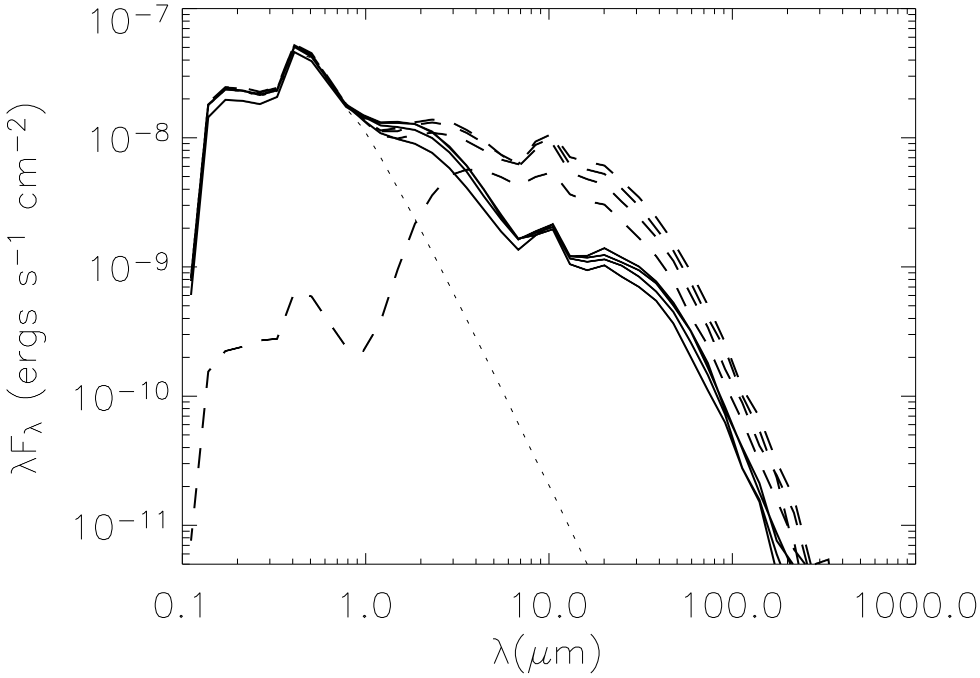

Fig. 4.— SEDs for disk of mass $10^{-2}M\odot$ and with power law exponent $p = 4$. Hydrostatic models (solid lines) and fixed density models with $h_{dust} = 0.036R_\star$, $\beta = 1.35$ (dashed lines) are shown. Inclinations are: $72.5 - 75.5°; 60.0 - 63.3°; 45.6 - 49.5°; 25.8 - 31.8°$.

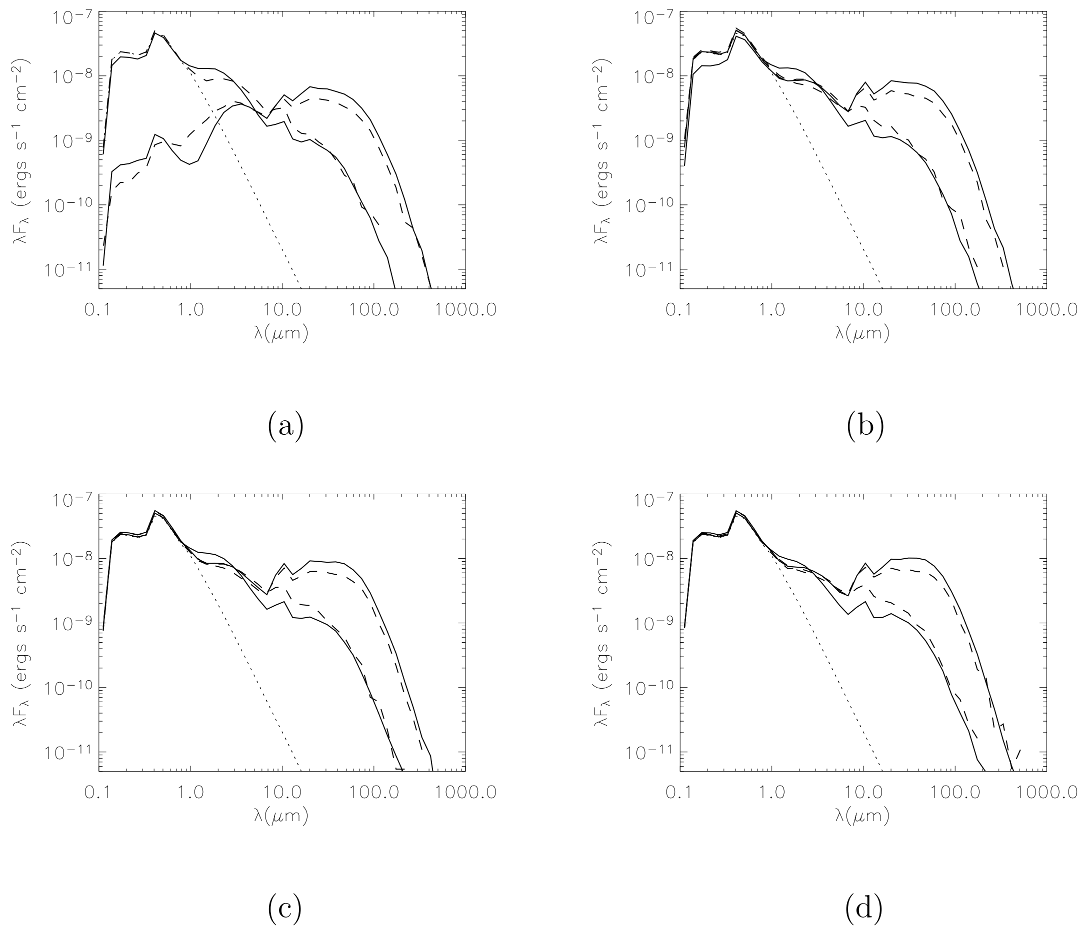

Fig. 5.— SEDs for hydrostatic disks of mass $10^{-2}M_{\odot}$ and with power laws p=1 and p=4. Hydrostatic models are shown as solid lines and fixed density models as dashed lines. All fixed density models have $h_{dust} = 0.036R_{\star}$ and $\beta = 1.25$. Inclinations are: (a) $i = 72.5–75.5°$; (b) $i = 60.0 - 63.3°$; (c) $i = 45.6 - 49.5°$; (d) $i = 25.8 - 31.8°$.

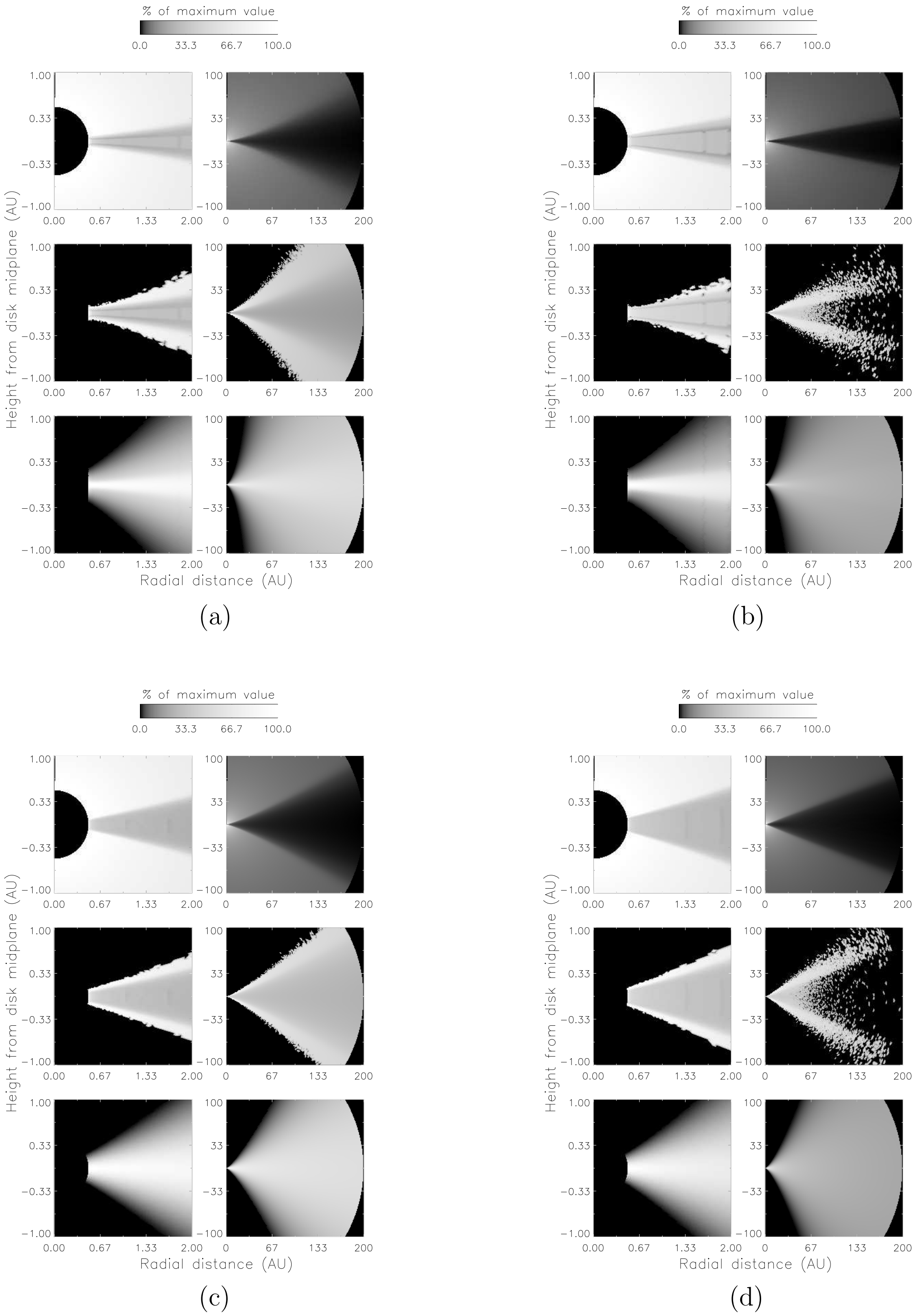

Fig. 6.— 2D temperature and density slices on two sizescales for hydrostatic and fixed passive disks of mass $10^{-2}M\odot$ with varying surface density: (a) $Hydrostatic, p = 1$; (b) $Hydrostatic, p = 4$; (c) $Fixed, p = 1, h_{dust} = 0.036R_{\star}, \beta = 1.25$; (d) $Fixed, p = 4, h_{dust} = 0.036R_{\star}, \beta = 1.35$. Each set of plots show temperature (upper and middle) and density. Data presented on a logarithmic scale.

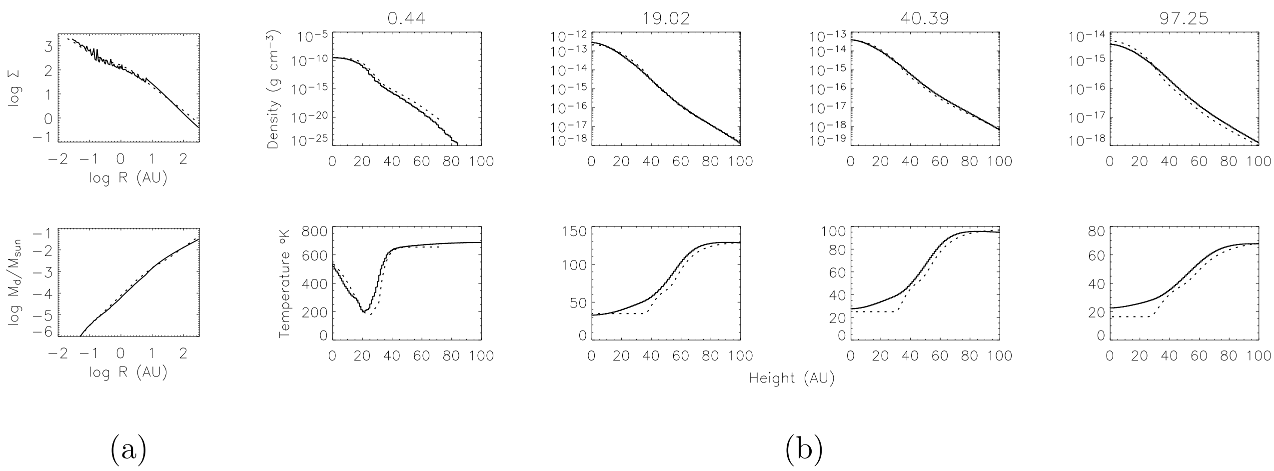

Fig. 7.— Cross-sections through a hydrostatic disk model (solid lines) and through a vertical-only model of the same parameters (dotted). Central star has $T_\star = 4000K$, $R_\star = 2R_\odot$, $M_\star = 0.5M_\odot$. Disk parameters and features: (a) mass surface density and cumulative mass profiles for radial transport (solid) and vertical-only (dotted) model, where disk extends from $3R_\star$ to 300AU; (b) horizontal sets of panels showing temperature(upper) and density (lower) at a fixed radial distance from the central star (given in AU above each set of plots).

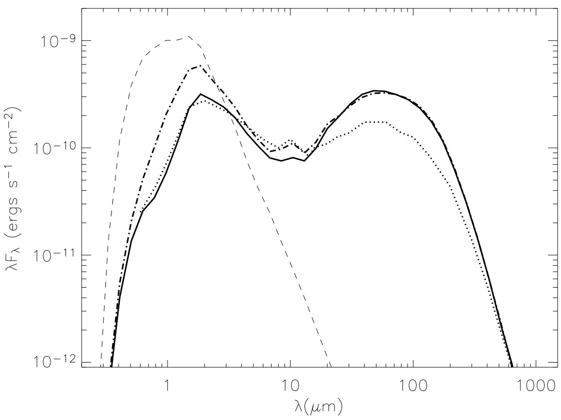

Fig. 8.— SED for a vertical-only model at $i = 60°$ (dotted) compared with radial transport model at $i = 60°$ (dash-dot) and $i = 63°$ (solid). Parameters as in Fig. 7.

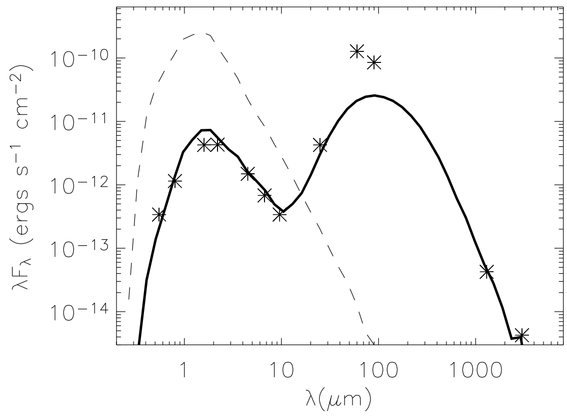

Fig. 9.— SED model fit to HH30 data from Mundt & Fried (1983:V and I); Vrba, Rydgren, & Zak (1985: H,K, and an upper limit at L); Reipurth et al (1993: 1.3mm) and Stapelfeldt & Moneti (1999: 4.5 - 90 microns). Model is for a 250AU disk inclined at 81°. Model SED has been reddened by Av=2 and disk is assumed to be at 140pc. Other parameters are: $\dot{M} = 2 \times 10^{-9} M_\odot$ yr^{-1}, M_d = 3x$10^{-3} M_\odot$, $T_\star = 3500K$, $R_\star = 1.5 R_\odot$, $M_\star = 0.64 M_\odot$, $R_{in} = 5R_\star$.

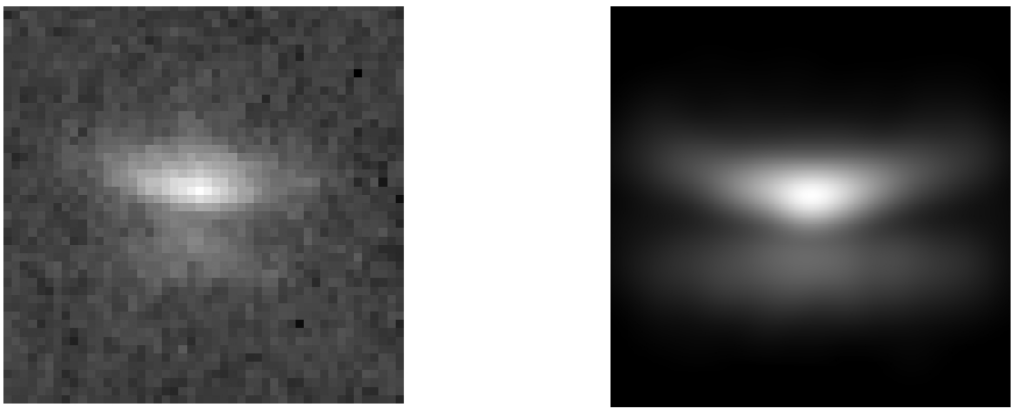

Fig. 10.— K-band model (right) and data image (left) for HH30 data. Model parameters are as for Fig. 9

REFERENCES

Acke, B., & van den Ancker, M. E. 2004, A&A, 426, 151

Akeson, R. L., et al., 2005, ApJ, 622, 440

Bell, K. R., Cassen, P. M., Klahr, H. H., & Henning, Th., 1997, ApJ, 486, 372

Bjorkman, J. E., Whitney, B. A., & Wood, K., 2003, BAAS, 34,

Bjorkman J. E., & Wood K., 2001, ApJ, 554, 615

Bouvier J. et al., 1999, A&A, 349, 619

Burrows, C. J., et al. 1996, ApJ, 473, 437

Calvet, N., Patino, A., Magris, G. C., & D'Alessio, P. 1991, ApJ, 380, 617

Chiang, E. I., & Goldreich, P. 1997, ApJ, 490, 368

——— 1999, ApJ, 519, 279

Chiang E. I., Joung M. K., Creech-Eakman M. J., Qi C., Kessler J. E., Blake G. A., & van Dishoeck E. F., 2001, ApJ, 547, 1077

Cotera A. et al., 2001, ApJ, 556, 958

D'Alessio, P., Cantó, J., Calvet, N., & Lizano, S., 1998, ApJ, 500, 411

D'Alessio, P., Calvet, N., Hartmann, L., Lizano, S., & Cantó, J., 1999, ApJ, 527, 893

D'Alessio, P., Calvet, N., & Hartmann, L. 2001, ApJ, 553, 321

D'Alessio, P., Merlín, B., Calvet, N., & Hartmann, L., 2005, RMxAA, 41, 61

Dullemond, C. P. 2002, A&A, 395, 853

Dullemond, C., & Dominik, C. 2004, A&A, 417, 159

Dullemond, C. P., Dominik, C., & Natta, A., 2001, ApJ, 560, 957

Grosso, N., Alves, J., Wood, K., Neuhäuser, R., Montmerle, T., & Bjorkman, J.E. 2003, ApJ, 586, 296

Gullbring, E., Hartmann, L., Briceño, C., & Calvet, N. 1998, ApJ, 492, 323

Hartmann, L., Calvet, N., Gullbring, E., & D'Alessio, P. 1998, ApJ, 495, 385

Kenyon, S. J., & Hartmann, L., 1987, ApJ, 323, 714

Kessler-Silacci, J. E., Hillenbrand, L. A., Blake, G. A., Meyer, M. R., 2005, ApJ, 622, 404

Kim, S. H., Martin, P. G., & Hendry, P. D., 1994, ApJ, 422, 164

Krist, J. E., Clampin, M., Golimowski, D. A., Ardila, D. R., Ford, H. C., & Illingworth, G. D., 2003, IAUS , 221P, 125K

Krist, J. E., et al., 2005, ApJ, 129, 1008

Kurosawa R., Harries T. J., Bate M. R., & Symington N. H., 2004, MNRAS, 351, 1134

Lucy L. B., 1999, A&A, 344, 282

Mendoza, E. E. V., 1968, ApJ, 151, 977

Ménard, F., Bouvier J., Dougados C., Melnikov S. Y., & Grankin K. N., 2003, A&A, 409, 163

Natta, A., Meyer, M. R., & Beckwith, S. V. W. 2000a, ApJ, 534, 838

Natta, A., Prusti, T., Neri, R., Grinin, V. P., & Mannings, V., 2001, A&A, 371, 186

Nomura, H., 2004, Ap&SS, 292, 435

Muzerolle, J., D'Alessio, P., Calvet, N., & Hartmann, L., 2004, ApJ, 617, 406

O'Sullivan, M., Truss, M., Walker, C., Wood, K., Matthews, O., Whitney, B., & Bjorkman, J. E., 2005, MNRAS, 358, 632

Padgett, D. L., Brandner, W., Stapelfeldt, K. R., Strom, S. E., Terebey, S., & Koerner, D. 1999, AJ, 117, 1490

Pascucci, I., Wolf, S., Steinacker, J., Dullemond, C. P., Henning, T., Niccolini, G., Woitke, P., & Lopez, B., 2004, A&A, 417, 793

Pringle, J. E., 1981, ARA&A, 19, 137

Author(s). 2000, in Protostars and Planets IV, ed. V. Mannings, A. P. Boss, and S.S. Russell (Tucson: Univ. Arizona Press), 355

Rice, W. K. M., Wood, K., Armitage, P. J., Whitney, B. A., & Bjorkman, J. E. 2003, MNRAS, 342, 79

Schneider, G., Wood, K., Silverstone, M. D., Hines, D. C., Koerner, D. W., Whitney, B. A., Bjorkman, J. E., & Lowrance, P. J., 2003, AJ, 125, 1467

Shakura N. I., & Sunyaev R. A., 1973, A&A, 24, 337

Shu, F. H., Adams, F. C., & Lizano, S., 1987, ARA&A, 25, 23

Stapelfeldt K. R. et al., 1999, ApJ, 516, L95

Steinacker, J., Lang, B., Burkert, A., Bacmann, A., & Henning, Th., 2004, ApJ, 615, L157

Walker, C., Wood, K., Lada, C. J., Robitaille, T., Bjorkman, J. E., & Whitney, B., 2004, MNRAS, 351, 607

Watson A. M., & Stapelfeldt K. R., 2004, ApJ, 602, 860

Weinberger, A. J., et al. 2002, ApJ, 566, 409

Whitney, B. A., & Hartmann, L. 1992, ApJ, 395, 529

Whitney, B. A., Wood, K., Bjorkman, J. E., & Cohen, M. 2003, ApJ, 598, 1079 (Paper II)

Whitney, B. A., Indebetouw, R., Bjorkman, J. E., & Wood, K., 2005, in press

Wolf, S. 2001, A&A, 379, 690

Wood, K., Kenyon, S. J., Whitney, B., & Turnbull, M., 1998, ApJ, 497, 404

Wood, K., Wolff, M. J., Bjorkman, J. E., & Whitney, B., 2002, ApJ, 564, 887

Wood K., & Whitney B. A., 1998, ApJ, 506, L43

Wood, K., Wolk, S. J., Stanek, K. Z., Leussis, G., Stassun, K., Wolff, M., & Whitney, B., 2000, ApJ, 542, L21

This manuscript was prepared with the AAS LATEX macros v5.0.